

Cite this: *Phys. Chem. Chem. Phys.*, 2011, **13**, 8331–8344www.rsc.org/pccp

PAPER

Stereocontrol of attosecond time-scale electron dynamics in ABCU using ultrafast laser pulses: a computational study^{†‡}

B. Mignolet,^a A. Gijsbertsen,^b M. J. J. Vrakking,^{*bc} R. D. Levine^{*de} and F. Remacle^{*ad}

Received 11th January 2011, Accepted 23rd March 2011

DOI: 10.1039/c1cp20094a

The attosecond time-scale electronic dynamics induced by an ultrashort laser pulse is computed using a multi configuration time dependent approach in ABCU ($C_{10}H_{19}N$), a medium size polyatomic molecule with a rigid cage geometry. The coupling between the electronic states induced by the strong pulse is included in the many electron Hamiltonian used to compute the electron dynamics. We show that it is possible to implement control of the electron density stereodynamics in this medium size molecule by varying the characteristics of the laser pulse, for example by polarizing the electric field either along the N–C axis of the cage, or in the plane perpendicular to it. The excitation produces an oscillatory, non-stationary, electronic state that exhibits localization of the electron density in different parts of the molecule both during and after the pulse. The coherent oscillations of the non-stationary electronic state are also demonstrated through the alternation of the dipole moment of the molecule.

1. Introduction

The development of ultrashort, attosecond and few-femtosecond laser pulses has in the last few years opened new avenues towards the probing and controlling of molecular electron dynamics, and thereby of the controlling of molecular reactivity.^{1–4} Using attosecond laser pulses generated by means of high-harmonic generation, pump–probe experiments can be configured where electron dynamics is monitored on its natural—attosecond—time-scale.^{5–8} In high-harmonic generation, an intense femtosecond laser ionizes an atomic or molecular gas, accelerates the electrons thus produced, and then drives them back towards the ions left behind. The electron–ion re-collision produces attosecond laser pulses,¹ and additionally allows the imaging of both structural and electronic dynamics of the ion on the attosecond to few-femtosecond timescale.^{9,10} For example, ultrafast electron migration processes¹¹ and

the onset of molecular dissociation¹² have both been inferred in the short time interval between the departure of the electron and its return to the ion. Finally, using few-femtosecond laser pulses with a stable carrier envelope phase (CEP), it has been shown that charge densities in molecules can be controlled and localized on the attosecond time-scale.^{13,14}

So far, most of these experiments have been performed in small, primarily diatomic molecules. For example, a first molecular attosecond pump–probe experiment was recently performed for H_2 and D_2 ,⁸ and this was also the system where electron localization using a CEP-stable laser pulse was first demonstrated.¹³ The former experiments revealed two mechanisms for the localization of the electron density, involving both a coupling of purely electronic degrees of freedom and a coupling of electronic and nuclear degrees of freedom, with the interaction with an intense few-femtosecond IR pulse during the ionization and fragmentation of the ion playing an important role. Different variants of the high-harmonic imaging technique have thus far also primarily been used to study small molecules like N_2 ^{10,15} CO_2 ^{11,16} and Br_2 .^{17,18} Related experiments where electrons rather than harmonics are measured have recently been reported as well.^{19–21}

We report in this paper on a computational study on electron density localization during and after excitation by a few-fs intense laser pulse in a medium-size molecule, ABCU ($C_{10}H_{19}N$) with a rigid cage, see Fig. 1. The neutral equilibrium geometry of ABCU belongs to the C_3 point group. Because of the rigidity of the ABCU cage, the geometry of the ground state is maintained in the dipole-allowed excited states with very little nuclear rearrangement. At the geometry of

^a Department of Chemistry, University of Liège, B4000 Liège, Belgium. E-mail: fremacle@ulg.ac.be

^b FOM-Institute AMOLF, Science Park 104, 1098 XG Amsterdam, The Netherlands. E-mail: marc.vrakking@mbi-berlin.de

^c Max-Born-Institut, Max Born Straße 2A, D-12489 Berlin, Germany

^d The Fritz Haber Center for Molecular Dynamics, The Hebrew University of Jerusalem, Jerusalem 91904, Israel. E-mail: rafi@huji.ac.il

^e Department of Chemistry and Biochemistry and Department of Molecular and Medical Pharmacology and Crump Institute for Molecular Imaging, The University of California Los Angeles, Los Angeles, CA 90095

† Electronic supplementary information (ESI) available. See DOI: 10.1039/c1cp20094a

‡ Presented at the XIII Stereodynamics meeting, Santa Cruz, November 2010.

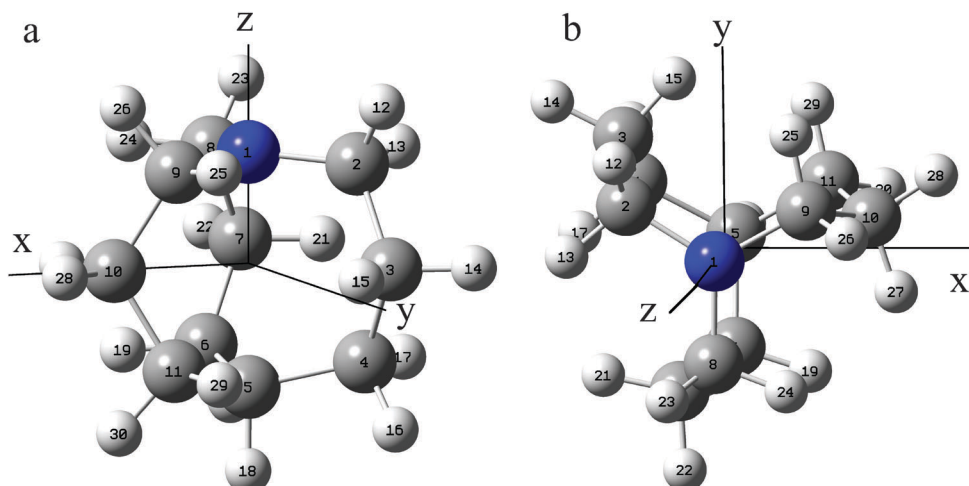


Fig. 1 Equilibrium geometry of ABCU computed at the CAS(8,13)/6-31++G(d,p) level. ABCU belongs to the C_3 symmetry group. The Cartesian frame attached to the center of mass is also shown. In the standard orientation, the C_3 axis is along the z Cartesian axis, and passes by the N and C_5 atoms, while the x and y axis are perpendicular to it with the $C_9-C_{10}-C_{11}$ arm being roughly aligned in the (z,x) plane. The middle carbon atoms of each of the three arms, C_3 , C_7 and C_{10} respectively are in the (x,y) plane. (a) View with a vertical z axis. This view emphasizes the $N-C_5$ axis and is used below to visualize the electron motion along this direction. (b) View of the cage from the positive z direction. This view is used below to visualize the electron motion in the (x,y) plane, in the direction perpendicular to the $N-C_5$ axis. The extension of the cage along the z axis, from the N to the C_5 atom is 3.088 Å while the distance between two carbon atoms in the (x,y) plane is 3.631 Å.

the neutral, these UV-accessible excited states are essentially stable and do not have imaginary frequencies, so that no significant nuclear dynamics should take place during the excitation by an ultrafast pulse.

We show that the electron localization can be controlled by varying the polarization of the pulse with respect to the orientation of the molecule and by choosing the excitation wavelength, which can be resonant with the lowest excited states and in the UV range, or non-resonant, in the IR range. In addition, the electron localization depends on the duration of the pulse. We report computational results below using two pulse durations, namely an ultrashort pulse with a pulse duration equal to 1.16 fs FWHM and a pulse with a FWHM pulse duration of 2.33 fs. The short pulse allows for more selectivity, in particular for the IR excitation wavelength where it is a one cycle pulse, and where the results are sensitive to the value of the CEP. While on the edge of what can experimentally be achieved in the UV, such short pulses have not yet been produced in the IR. The longer pulse is in the range of what has been demonstrated experimentally.^{22–24} Except for the role of the CEP phase value for the short IR pulse, the results are not very much dependent on the pulse duration, as long as the pulse remains a few-cycle pulse.

We report that, by ultrafast excitation, not only is the excited state localized but that the corresponding electron density can also be oriented in space. Both the localization and its orientation are time-dependent and evolve with characteristic frequencies that are typical of the excitation frequency and also of the spacings between the excited states. The latter can be significantly lower than the excitation frequency and therefore the non-equilibrium electron dynamics can not only be probed during the laser excitation but also after the exciting laser pulse is over.

The electronic states of ABCU in the C_3 geometry belong either to the A symmetry (analogous to the Σ symmetry of a

diatomic molecule) or to the doubly degenerate E symmetry that is analogous to the Π states. Moreover, due to the asymmetry between the N (top) and C_5 (bottom) part of the cage (see Fig. 1), ABCU behaves as a hetero-nuclear diatomic molecule but with a larger span of about 3 Å. Two wavelengths are investigated in the simulations, an IR 800 nm wavelength typical of the Ti-Sapphire laser and a wavelength of 253 nm that can access the excited states of the neutral ABCU molecule by a one-photon transition. At the excitation wavelengths and field strengths investigated, we remain below the IP and the threshold for fragmentation. The ABCU molecule is therefore a very attractive molecule to explore purely electronic dynamics and to investigate how electronic motion can be controlled before the onset of the coupling of the electronic degrees of freedom to the nuclear degrees of freedom.

We show that ultrafast excitation produces a localized and non-stationary electronically excited density that can also be described as a coherent superposition of stationary states. Furthermore, we show that by suitably tailoring the excitation pulse it is possible to achieve a spatial directional control of the electron dynamics. When the polarization of the pulse is parallel to the $N-C_5$ axis of the molecule, see Fig. 1, one can induce a localization of the electron density alternatively at the N and at the C_5 end of the molecule during one optical cycle by building a superposition of A excited states with opposite permanent dipole moments. By polarizing the pulse in the (x,y) plane, that is perpendicular to the $N-C_5$ axis, one can induce a rotation of the electron density in that plane. The time dependence of the localization of the electron density in the different parts of the molecule is probed by following the electron density in real space and by computing the time-dependence of the components of the dipole moment. Experimentally, provided that the molecule can be oriented along the Cartesian axis shown in Fig. 1, the motion of the electron

Table 1 Excitation energies (eV) and components of the permanent (μ) and transition dipole moment, μ_{GS-ES} (a.u.) in the Cartesian frame shown in Fig. 1. The values are computed at the CAS average (8,13)/6-31++G(d,p) level for 19 states for the equilibrium geometry of the neutral. The energies and components of the permanent dipole moment of the cation computed at the CAS(7,13)/6-31++G(d,p) level are also reported

Excitation energy/eV	Symmetry	μ (a.u.)			μ_{GS-ES} (a.u.)		
		x	y	z	x	y	z
GS	A	-0.01	0.00	-0.44			
ES 1	A	0.00	0.00	-4.13	0.00	0.00	0.06
ES 2	E	0.66	0.21	-1.51	0.65	0.38	0.00
ES 3	E	-0.66	-0.22	-1.53	-0.39	0.65	0.00
ES 4	A	0.03	0.02	3.84	0.00	0.00	-0.28
ES 5	E	1.36	0.18	0.34	-0.06	0.26	0.00
ES 6	E	-1.37	-0.19	0.35	-0.26	-0.07	0.00
ES 7	E	0.17	1.00	3.93	-0.13	-0.13	0.00
ES 8	E	-0.20	-1.03	3.99	0.13	-0.13	0.00
ES 9	A	-0.04	0.00	5.70	0.00	0.00	0.07
CATION	A	0.00	0.00	1.38			
ES 10	E	-0.72	-0.28	3.63	0.15	0.08	-0.05
ES 11	E	0.69	0.28	3.59	-0.08	0.15	0.00
ES 12	A	0.09	0.03	3.62	-0.02	-0.01	-0.35
ES 13	A	0.30	-0.03	0.23	-0.14	-0.03	-0.13
ES 14	E	-0.44	-0.24	0.33	-0.04	0.23	0.00
ES 15	E	-0.41	-0.06	0.28	0.24	0.05	-0.08
ES 16		0.46	0.23	0.16	-0.04	0.15	-0.01
ES 17		0.69	0.42	-2.18	0.03	-0.04	0.01
ES 18		-0.53	-0.29	-1.56	0.07	-0.05	0.00

density could be probed by sudden ionization of the molecule with ultrashort XUV pulses and measuring the angular pattern of the ionized electron. While recent experiments suggest that it is reasonable to assume that the molecules can be oriented along the N–C₅ axis,^{25,26} it will be experimentally much more challenging to control the orientation of the three arms of the molecule. As illustrated by the computational examples discussed below, orienting the molecules along the N–C₅ axis would allow to probe the major effect in the electron localization, that is the electronic motion occurring along the N–C₅ axis or in the plane perpendicular to it. We also show that the control of the orientation of the arms would allow to preferentially access a given E state.

2. Electronic structure of the ground and the excited states of ABCU

The properties of the stationary field free states of the ABCU (ground state, GS, and excited states) were studied at the MC-SCF level^{27,28} using the program MOLPRO.²⁹ Several active spaces and basis sets were investigated in order to verify the stability of the results. We selected a complete active space (CAS) of 8 electrons and 13 molecular orbitals (4 occupied and 9 unoccupied in the GS) (8,13) with the 6-31++G(d,p) Gaussian basis set. This leads to an active space of 143 143 CSFs (Configuration State Functions).

The equilibrium geometry of the ground state (GS) of the neutral was optimized at this level and is shown in Fig. 1. The geometry is not constrained to be of C₃ symmetry but the C₃ symmetry is obtained after geometry optimization. We also obtain a very similar C₃ symmetry at the Hartree–Fock and B3LYP levels using the same basis set. The presence of diffuse functions in the basis set is important to describe correctly the electron density on the N atom. The geometry of the cation was also optimized at the CAS (8,13), HF and DFT/B3LYP

levels using the same basis set. The C₃ geometry is preserved upon ionization and upon relaxation, and we observe very small geometry changes, the main one being a more planar character of the N–C bonds at the top and a subsequent decrease of the extension of the cage along the z axis (see Fig. 1). The computed vertical and adiabatic ionization potentials (IP) are too low at the CAS and HF level but the values at the B3LYP level compare well with the experimental ones.³⁰ We also note that the computed vertical and adiabatic IP values are very close, in agreement with the close adiabatic and diabatic measured IP values.³⁰ The cation at the geometry of the neutral has no imaginary frequencies at the HF/6-31++G(d,p) level and at the DFT-B3LYP/6-31++G(d,p) level. We obtain 5.99 eV and 5.76 eV for the vertical and adiabatic CAS IPs respectively, 5.96 and 5.64 at the HF level and 6.96 and 6.80 at the B3LYP level compared to 7.01 vertical and 6.94 adiabatic experimentally.³⁰

A CAS averaged computation at the (8,13)/6-31++G(d,p) level was then performed for the 19 lowest excited states of the neutral for the GS geometry. Among the 19 states, 10 states are below the vertical IP, computed to be 5.99 eV at the CAS level. The 10 states below the IP are 4 A states (GS and three excited A states) and 3 doubly degenerate excited E states. The energies of the excited states computed at the optimized geometry of the neutral are reported in Table 1. They compare well with a previous *ab initio* study of ABCU at the SAC-CI level³¹ and with the experimental adiabatic excitation energies measured by Parker.³² The good agreement between the computed vertical excitation energies and the adiabatic ones reported in ref. 32 confirms the very low level of nuclear relaxation of the excited states. We investigated the stability of the lowest excited states and we find that the two lowest excited A states and the lowest E state are stable (no imaginary frequencies) at the geometry of the neutral at the TD-DFT level and the four A states are also stable at the CIS level.

Table 2 Components of the dipole moment. Top: for the three lowest excited states at the geometry of the neutral (left) and for the geometry optimization of the state for a CAS average (2,5)/6-31++G(d,p) computation. Bottom: for the cation, at the geometry of the neutral (left) and for the equilibrium geometry (right) computed at the CAS (7,13)/6-31++G(d,p)

μ (a.u.)						
	Equilibrium geometry of the GS			Optimized geometry		
State	x	y	z	x	y	z
1st A	0.00	0.00	-1.25	0.00	0.00	-1.55
1st E	0.78	-1.20	-0.11	1.01	-1.33	-0.08
2nd A	0.00	0.00	4.18	0.00	0.00	3.70
Cation	-0.04	-0.02	1.37	0.01	-0.04	1.36

When the geometry of the excited states is relaxed at the same level, we hardly observed any geometry changes and the C_3 geometry is preserved. The most significant geometry change for the 4 lowest excited states is a decrease of the N–C₅ elongation of the cage (from 3.115 to 2.990 Å for a geometry optimization with a smaller active space CAS average (2,5)/6-31++G(d,p)). The decrease in the N–C₅ extension of the cage in the case of the cation for a geometry optimization at the CAS(8,13)/6-31++G(d,p) level is from 3.089 Å in the neutral GS to 2.990 Å. We also observe an increase of the planarity of the N–C bonds at the top of the molecule: the angle C₉NC₂ is increasing from 119.35° in the GS to 119.97° in the cation for geometry optimization at the CAS(8,13)/6-31++G(d,p) level. These geometry changes are summarized in Table 2. They reflect a variation of the electron density at the N atom. When the bonding pattern at the N becomes more planar, the electron density on the N becomes less.

Due to the small nuclear reorganization of the excited states, the values of the components of the permanent dipole for the equilibrium geometry of the excited states is very close to that of those computed at the geometry of the neutral. They are given in Table 2.

For nuclei clamped at the equilibrium geometry of the neutral, the promotion of electrons into unoccupied MOs leads to a change in the electronic density that is reflected in the values of the components of the electronic permanent dipole. The nuclear contribution to the permanent dipole moment computed at the equilibrium geometry of the neutral is $\mu_x = 0.002$ a.u., $\mu_y = 0.023$ a.u. and $\mu_z = 1.612$ a.u. Since the nuclei are clamped, the nuclear contribution to the dipole is the same for all the excited states. The changes in the electron density lead to an inversion of the component of the permanent dipole moment along the z direction of the 2nd excited A state which becomes positive, compared to the GS and the 1st excited A state which have a negative permanent dipole moment. The reorganization of the electron density in the excited states also affects the values of the transition dipole moment, which is significantly larger from the GS to the 2nd A state than to the first one, see Table 1 for the numerical values. As a general rule, the transition moment to the A states is however about a factor 5 to 10 smaller than to the 1st E state, in agreement with the results of ref. 31. The CAS average computation gives access to the full matrix of the transition dipole for the band of 19 states included in the computation.

They are reported for the three polarization directions in Table S1 of the supporting information (ESI).†

The amplitudes on the CSFs of the excited states larger than a threshold of |0.05| are reported in Table S2 of the ESI.† The CSFs are expressed in the averaged natural orbitals that diagonalize the average density matrix. The 13 averaged natural orbitals of the active space are given in Fig. 2. They are clearly of A and E symmetry and their isocontours very similar to those of the HF and Kohn–Sham B3LYP orbitals, not shown. The active occupied MO (MO 40 to MO 43) are delocalized over the entire cage while the unoccupied ones are more clearly localized either on the N (MO 50) or the bottom C atom (MO 44, LUMO) or on the C skeleton (45 and 46, E and 48 and 49, E).

The excited states below the IP are composed of one or two main singly excited CSFs, from the HOMO (MO 43, A symmetry localized on the N and the top of the cage) to unoccupied MOs. The reason is that there is a significant gap (of 3.13 eV at the HF level and 3.07 eV at the DFT level) between the HOMO and the HOMO-1 and HOMO-2 which are the two components of a MO of E symmetry. The 1st excited A state is made of two CSFs with an excitation from HOMO to the MO 47 (basically a 4S of the N atom) and to the MO 50 (localized in the N and on the top C carbons). The two components of the first excited E state are also made of two CSFs, with an excitation of the HOMO to the MO 45 and 46 which correspond to the 2p_x and 2p_y orbitals of the C atoms in the arms and have no weight on N and to MO 51 and 52 which have a weight on the 3p_x and 3p_y AO of N. The second excited A state which has a positive permanent dipole moment along z is made of the superposition of two CSFs, which correspond to the excitation from the HOMO to the LUMO, localized on the bottom C₅ atom and to MO 50, localized on the N atom. The two components of the next E state are made of a single CSF, corresponding to the excitation from the HOMO to MO 48 and 49 respectively, which have a significant weight on

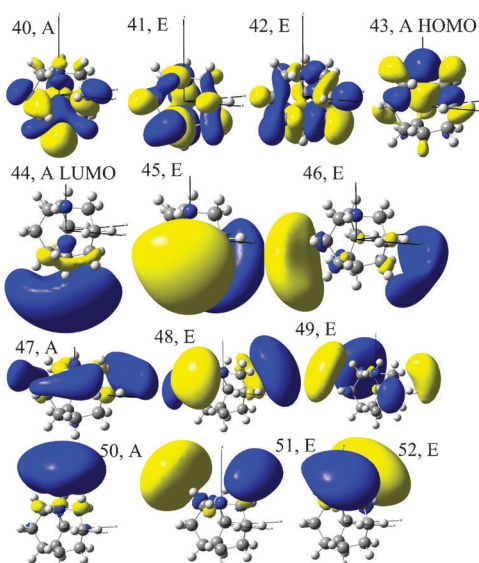


Fig. 2 Isocontours (isovalue of 0.02 |e|/Å³) of the 13 average natural orbitals corresponding to the active space of the CAS (8,13)/6-31++G(d,p) computation for a band of 19 states.

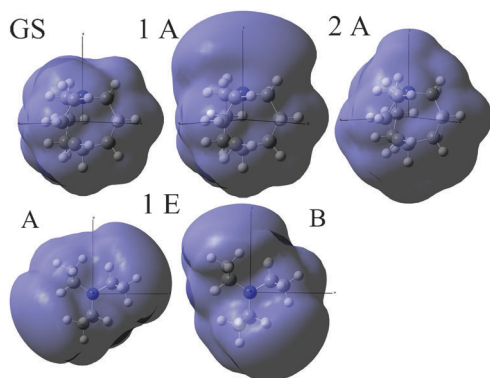


Fig. 3 Isocontours of the stationary one electron density, ρ (isovalue $0.0003 \text{ |e| } \text{\AA}^{-3}$), for the GS and the 4 lowest excited states obtained from a CAS averaged (8,13)/6-31++G(d,p) on a band of 19 states. Note that the components A and B of the first E state are rotated by about $30\text{--}45^\circ$ with respect to the (x,y) axis.

the d orbital of the N. The nature of the excited states are in good agreement with the analysis made by Galasso in ref. 31. Isocontours of the one electron densities of the two lowest excited states of A and E symmetry as well as for the GS are shown in Fig. 3. In a many-electron system (in ABCU 86 in total), differences in occupation of the MOs of the different CSFs contributing to the excited states are often somewhat smeared when plotting isocontours of the one electron density. In ABCU, because of the different symmetry of the A and the E states and of the presence of the N atom, some differences are however significant. We can see that for the GS and the first A state, there is more electronic density at the N part of ABCU while for the 2nd A state, there is more electron density at the bottom. The components of the E state correspond to an accumulation of density in the plane perpendicular to the z axis, at an angle of $30\text{--}45^\circ$ compared to x and y Cartesian axis. These trends in the electron densities reflect the excited MO in the CSFs. They significantly affect the value of the dipole moment, which is an average over the one electron density.

Since all the CSFs that have a significant amplitude are singly excited, we also performed a CIS(D)/6-31++G(d,p) computation of the excited states at the geometry of the neutral using the implementation of Gaussian 09.³³ We basically obtain the same trends in the values of the permanent and transition dipole moments (see Table S3 of the ESI)† for the 10 states below the IP, computed at the same equilibrium geometry of the GS as the one used for the CAS computation. The same energetic order for the lowest 6 excited states below the IP (the highest E and A state being quasi degenerate) is recovered, however, the excitation energies, which in the CIS(D) approach are corrected perturbatively do not agree as well with the experimental ones than the ones computed at the CAS level.

In what follows we pay special attention to the orientation of the molecule with respect to the laser field because it is likely that the stereodynamical control of the electron density motion that we aim to experimentally demonstrating in the future will average out for a randomly oriented sample of molecules. Since a few years, techniques for the alignment of molecules are available,³⁴ where molecules are exposed to a

moderately strong ($\sim 10^{12} \text{ W cm}^{-2}$) non-resonant laser field during (adiabatic alignment, see ref. 35) or prior to (non-adiabatic alignment, see ref. 36) the experiment. More recently, these techniques have been extended towards orientation of molecules. By combining hexapole state-selection, orientation in a DC electric field and exposure to the field of a shaped laser pulse, an orientation characterized by $\langle \cos^2 \theta \rangle = 0.74$, with θ the angle between the molecular axis and the laser polarization axis, was achieved for NO molecules.²⁵ Larger polar molecules, such as iodobenzene, have been oriented following state-selection making use of an electro-static deflector, which also provides a method to separate structural isomers.²⁶

3. Static field effects

We first start by investigating the effect of a static field on the eigenenergies and eigenstates of the electronic Hamiltonian. The energies of the excited states as a function of the strength of a static field applied in the z and in the (x,y) plane are shown in Fig. 4. The effect of a static field is included in the electronic Hamiltonian in the dipolar approximation:

$$H^{\text{elec}} = H_0^{\text{elec}} - \mu \cdot \mathbf{E} \quad (1)$$

The matrix of the electronic Hamiltonian H^{elec} is diagonalized in the basis of the field free states of H_0^{elec} obtained by the CAS

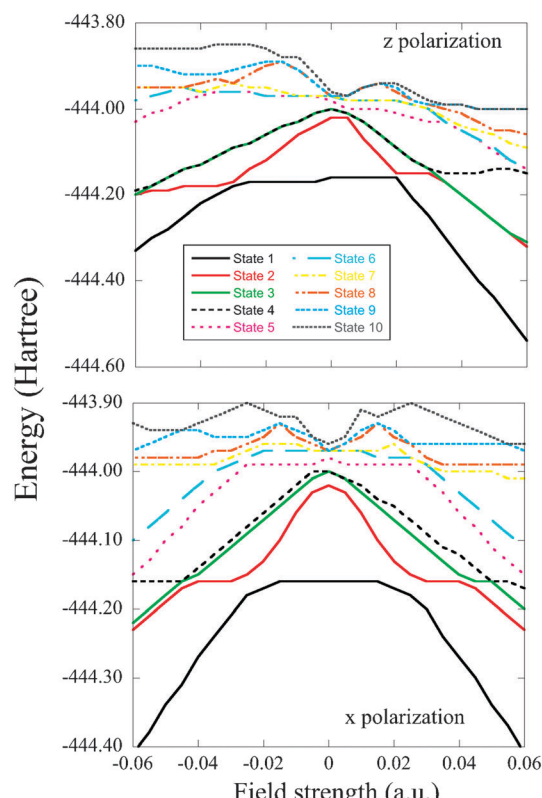


Fig. 4 Static field adapted energies as a function of the applied field strength computed as the eigenvalues of the electronic Hamiltonian (eqn (1)) for a z polarization of the static field (top panel) and for a x polarization (bottom panel). The directions x and z are the ones of the Cartesian frame in Fig. 1.

averaged computation. The matrix elements of the dipole matrix elements for the band of the 19 states at the equilibrium geometry of the neutral are reported in Table S1 of the ESI.[†] For a static field polarized in the z direction (Fig. 4 top panel), the states of A and E symmetry can cross because they are not mixed by the dipolar term. Due to the opposite sign of the dipole moment of the excited A states, the crossings are different in the positive and negative z direction of the applied field. When the applied field is polarized in the (x,y) plane (Fig. 4 lower panel), we also do not observe a perfect mirror symmetry because the two components of the E states are not aligned with the x and y Cartesian axis respectively.

Investigating the effect of a static field provides a semi-quantitative estimate of which kind of state mixing can be built when a strong oscillating field is applied. The estimate is only semi-quantitative because the electron density does not adjust adiabatically to the field strength, nor does it behave diabatically as was shown in detail in ref. 37 for the diatomic LiH molecule, and in ref. 38 for the two-color dissociative ionization of H₂ reported in ref. 8. This means that neither the field-free diabatic states (eigenstates of H_0^{elec}), nor the field adapted adiabatic states which are the eigenstates of the full electronic Hamiltonian (1) provide a good description of the electronic dynamics induced by a medium to strong oscillating electric field. It is therefore necessary to integrate numerically the time-dependent Schrödinger equation including the time-dependent electric field as explained below. The band of states must be large enough to describe the transient dynamics occurring during the pulse.

4. Electron dynamics

Several approaches have been proposed to compute electron dynamics in strong fields. Multi-Configurational (MC) methods that allow to relax both the configuration interaction (CI) coefficients and the MOs during the time evolution are usually limited to small polyatomic systems because the equations of motion (EOM) for the MOs are highly non linear.^{39–48} For diatomic molecules with one or two electrons, one can also use a discrete value representation on a grid.^{49,50} For larger ionized systems, at a one electron level, a density functional approach was proposed⁵¹ as well as an approach based on the ADC scheme.⁵² We apply here a correlated, MC time-dependent approach for a medium size polyatomic molecule.^{53,54} A MC-SCF computation is used to define a large basis of field free electronic states. The time-dependent Schrödinger equation for the many electron Hamiltonian that includes the time-dependent laser-molecule interaction is then solved numerically in the field free basis of MC electronic states. The rigidity of the nuclear skeleton allows us to use a clamped nuclei computation. Otherwise, effects of nuclear motion must be included.^{14,55–58}

The pulse is taken to have a Gaussian envelop

$$\mathbf{E}(t) = \mathbf{E} \exp\left(\frac{-(t-t_0)^2}{2\sigma^2}\right) \cos(\omega t + \phi) \quad (2)$$

where $\mathbf{E} = (E_x \mathbf{x} + E_y \mathbf{y} + E_z \mathbf{z})$ defines the strength and the orientation of the electric field, σ is the width of the pulse,

ω the excitation frequency and ϕ the carrier envelop phase (CEP) which governs the overall phase between the optical cycle and the envelope. Calculations will be presented where the ABCU molecules were exposed to UV ($\omega = 0.18$ a.u., corresponding to a 253 nm wavelength) and IR ($\omega = 0.057$ a.u., corresponding to an 800 nm wavelength) light pulses, with two values of σ : an ultrashort value equal to 0.72 fs (corresponding to an electric field FWHM of 1.65 fs and an intensity FWHM of 1.16 fs) and one twice longer, with a intensity FWHM of 2.33 fs. The short pulse duration is beyond the present state of the art for the generation of laser pulses in the optical^{22,23} and UV²⁴ domain, where pulses of 2.6–2.8 fs have so far been achieved, but presently allows to more clearly show the potential for electronic control that can be achieved in larger molecules upon excitation by ultrashort laser pulses, in particular for the case of the IR excitation, for which it is a one cycle pulse. In that case, we define $\mathbf{E}(t)$ from the vector potential $\mathbf{A}(t)$, $d\mathbf{E}(t)/dt = (-1/c)d\mathbf{A}(t)/dt$, in order to make sure that there is no DC or low frequency component in $\mathbf{E}(t)$.⁵⁹ For the other pulses, we numerically checked that this is not the case when using the expression (2) for $\mathbf{E}(t)$. The FWHM of the longer pulse of 2.35 fs, is closer to what can presently be achieved experimentally.

The total wave function is written as a superposition of field free states, $|\Psi_i\rangle$ which are the MC-SCF averaged eigenstates of H_0^{elec} in eqn (1).

$$|\Psi(t)\rangle = \sum_{i=1}^{N=19} c_i(t) |\Psi_i\rangle \quad (3)$$

where $i = 1$ is the GS. The amplitude $c_i(t)$ are computed by numerical integration of the time-dependent Schrödinger equation

$$i\hbar \frac{dc(t)}{dt} = \mathbf{H}(t) \mathbf{c}(t) \quad (4)$$

where $\mathbf{H}(t)$ is the matrix of the electronic time-dependent Hamiltonian

$$H(t) = H_0^{\text{elec}} - \mu \cdot \mathbf{E}(t) \quad (5)$$

in the field-free states and $\mathbf{E}(t)$ is given by eqn (2). The matrix elements of the dipole for the band of 19 electronic field-free states are reported in Table S1 of the ESI.[†] The basis set used does not include a dense set of ionizing states. Our primary aim here is to show that excitation with spatial selectivity can be achieved for the states of the neutral below the IP with pulses that can be produced experimentally. For the parameters used here, significant ionization can occur during the pulse, which will require special techniques to selectively probe the excitation of the states of the neutral. We however expect that the stereodynamic control of the purely electronic dynamics that we computationally demonstrate below will not be quenched by the modulation in the population of the excited states due to the ionization process. Work is in progress in this direction.

Several approaches have been proposed to include ionization in computational approaches, either analytical,⁶⁰ based on grid methods^{49,61} or on the partitioning technique or using absorbing potentials.^{45,62–66} The systems investigated are

usually limited to 2 active electron systems for which ionization and the coupling between nuclear and electronic degrees of freedom can be readily included. The Keldysh parameters for the UV pulses used in the computation below vary between 2 and 6 and those for the IR pulses are of the order of 1. The mechanism for ionization is therefore a mixture of tunnel and multiphoton ionization.

The electronic motion is probed by following the time-dependent dipole moment, $\mu(t)$

$$\mu(t) = \langle \Psi(t) | \mu | \Psi(t) \rangle = \sum_{i,j} c_i^*(t) c_j(t) \mu_{ij} \quad (6)$$

where the μ_{ij} are the matrix elements of the dipole in the field free states.

We also show below iso contours of the electronic density, $\rho(t)$

$$\rho(x, y, z, t) = \sum_{i,j} c_i^*(t) c_j(t) \rho_{ij}(x, y, z) \quad (7)$$

where the diagonal elements ρ_{ii} are the one electron densities of the GS and the excited states and the ρ_{ij} are the transition matrices between the field free states.^{67–69}

We show in the computational results below that the time-dependence of the 3D isocontours of one electron density, $\rho(t)$, eqn (7) correlates well with the beatings of components of the dipole moment (eqn (6)) as should be since both the time evolution of both quantities depends on the same interference terms. However, the isocontours of $\rho(t)$ shown below also provide additional insights on the spatial distortion of the electron density during and after the pulse. For a many electron case, where $\rho(t)$ is a coherent superposition of several excited states, themselves being built of several configurations, the distortion is complex, in particular for the superposition of A states induced by a pulse polarized along the z direction. We therefore also show $\rho_{GS} - \rho(t)$ which reflects the densities of those MOs that are excited in the configurations of the excited states that have a significant coefficient at time t . This is particularly useful when the excited states are of a symmetry different than that the ground state, as is the case for an excitation pulse polarized in the x direction. Experimentally the shape of $\rho(t)$ is of considerable interest, since the probing with XUV/X-ray light that is required for a time-domain probing of the electron motion, will primarily address the electron density that is (instantaneously) located near atomic centers.

5. Stereo electron dynamics in ABCU

A pulse polarized along the z direction cannot mix the A and E states while a pulse polarized in the (x, y) plane does mix the two kinds of symmetry. The polarization of the pulse is therefore an essential knob in controlling the motion of the electronic density. We expect that in ABCU the selection rules will not be easily relaxed because we do not observe a departure of the equilibrium geometry of the excited states from the C_3 symmetry.

We first report on the stereo-selectivity in the electron dynamics obtained for a pulse polarized along the z direction. Our aim is to build a superposition of excited A states such

that a motion of the electron density is induced up and down the N–C₅ axis of the molecule, along the z direction. Since the 1st excited A state has a permanent dipole in the same direction as the GS, we need to access the 2nd excited A state which has a permanent dipole in the opposite direction, see Table 1. The 2nd excited A state also has a larger oscillator strength than the first one. To significantly populate the 2nd A state, we have used a rather high field strength of 0.05 a.u. ($8.75 \times 10^{13} \text{ W cm}^{-2}$) and a resonant excitation wavelength 253 nm (= 0.18 a.u. = 4.9 eV). In order to keep the population in neutral states close to the IP and above less than 1%, we have used a rather short pulse, with a value of σ in eqn (2) equal to 0.72 fs (30 a.u.). This corresponds to a width in energy of 5.7 eV and a pulse duration (FWHM) of 1.16 fs. The dynamics in the excited states induced by the pulse is computed using eqn (4) including the 19 states of the band reported in Table 1. The weights on the excited states are shown in Fig. 5. In spite of the rather high field strength, only 0.6% of the population is in the neutral states that lie above the IP at the end of the pulse. These states do not get populated significantly (<3%) during the pulse either. At the end of the pulse, a superposition of the GS (77.9%) and the 2nd A state (17.3%) is obtained. During the pulse, one can also see that due to the smaller value of the transition dipole and the opposite sign the dipole moment, the 1st excited A state as well as the 3rd A state are populated after the 2nd one with an amount of a few percents (1.6% and 2.7% respectively) in the superposition.

The beatings of the components of the dipole moment, $\mu(t)$, eqn (6) are shown in Fig. 6. The dipole moment not only varies in time during the laser excitation, but also after the laser pulse has turned off, when very pronounced oscillations in the z -component of the dipole moment occur. This modulation of the dipole is due to the interference terms in eqn (6) and is a natural consequence of the fact that the laser excitation has produced a coherent superposition of electronic states, which continues to evolve after the laser pulse is over. One can see that there is no variation of the components of the dipole

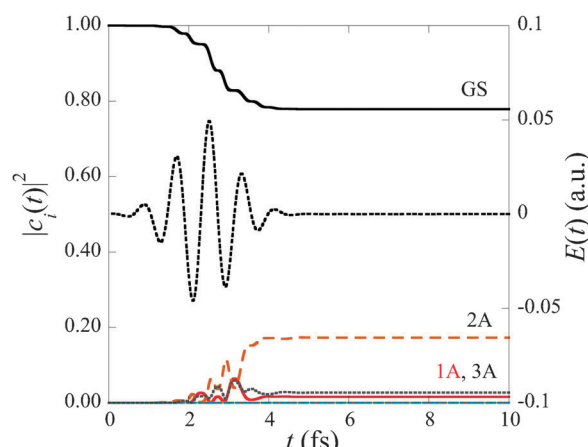


Fig. 5 Time evolution of the weights, $|c_i(t)|^2$, eqn (3), on the excited states for a pulse polarized in the $+z$ direction ($\omega = 0.18$ a.u., $|E| = 0.05$ a.u., $\sigma = 30$ a.u. and $\phi = 0$ in eqn (2)). The pulse is shown in dashes, scale on the right. Only A states are populated by a pulse polarized in the z direction.

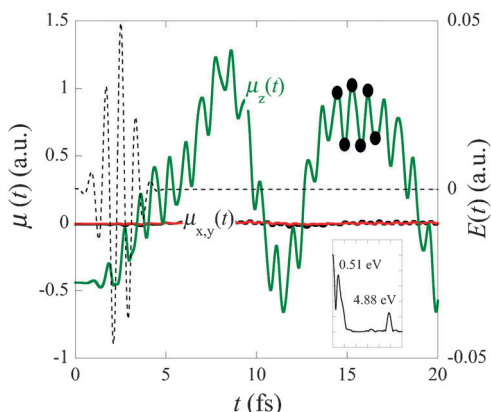


Fig. 6 Time-dependence of the components of the dipole moment, $\mu(t)$ (eqn (6)) computed for the pulse used in Fig. 5. The dots are the points in time at which isocontours of the density are shown in Fig. 7. Shown also as a dashed line is the excitation field, with the strength of the field shown on the right. A Fourier transform of the dipole moment is shown as an insert and shows the two groups of frequencies corresponding to the fast and slow beatings. The component at 4.88 eV reflects the energy difference between the GS and the 2nd A state. At low frequencies, two peaks are observed, corresponding to the energy difference between the 1st A state and the 2nd one (0.51 eV) and the energy difference between the 1st A state and the 3rd one (0.88 eV).

moment along x and y and that the component along z oscillates between -0.6 and $+1.5$ a.u. Also shown in Fig. 6 as an insert is the Fourier transform of the dipole moment in the z direction. One can see three frequencies, one at 4.88 eV which corresponds to the excitation energy of the 2nd excited A state (see Table 1) and governs the fast beating in the dipole moment. Two low frequency peaks correspond to the energy differences between the 1st excited A state and the 2nd one (0.51 eV) and between the 1st and the 3rd A state (0.88 eV).

Since the nuclei are clamped, the variation of the dipole is induced by the electronic motion only. We show in Fig. 7 isocontours of the difference of the one electron density at $t = 0$ ($= \rho_{GS}$) and $\rho(t)$ computed using eqn (7) at the time points shown in Fig. 6 for a time interval between 14.4 and 16.6 fs in which the electronic contribution to the dipole oscillates between -0.6 and -1 a.u., the value of the nuclear contribution along z being 1.6 a.u. The electronic motion is complex because a superposition of more than two states is built. In addition to the GS and the 2nd A state which dominate (see Fig. 5), there are components of the 1st and the 3rd excited A states in $|\Psi(t)\rangle$. The times chosen to show snapshots of $\rho(t)$ correspond to the fast beating between the GS and the 2nd A state and for these times, the oscillations of the one electron density is seen to be in agreement with those of the z component of the dipole. The dipole is less negative when there is less charge localized at the top of the molecule, around the N atom. One can also observe that for time when the dipole is less negative, the isocontours are much closer to the density of the stationary 2nd A state shown in Fig. 3 above. Fig. 8 shows the actual $\rho(t)$ computed at the first four time values shown in Fig. 7, 14.4, 14.9, 15.2 and 15.8 fs. The isocontours at the four time values have the same value of

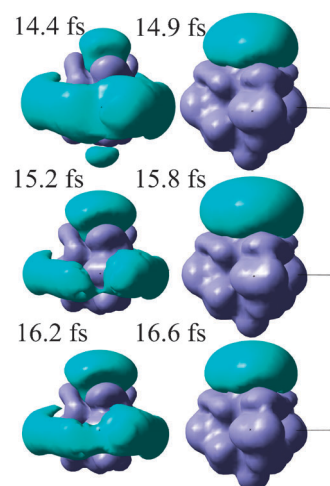


Fig. 7 Isocontours ($0.000055 |e|/\text{\AA}^3$) of $\rho_{GS} - \rho(t)$ computed for the excitation pulse used in Fig. 5. The value of μ_z^{elec} is -0.6 a.u. at $t = 14.4, 15.2$ and 16.2 fs and $\mu_z^{\text{elec}} = -1.0$ a.u. at $14.9, 15.8$ and 16.6 fs. There is not an exact recurrence at each oscillation because a superposition of states has been built at the end of the pulse. Green corresponds to an accumulation of electron density and violet to a default of electron density.

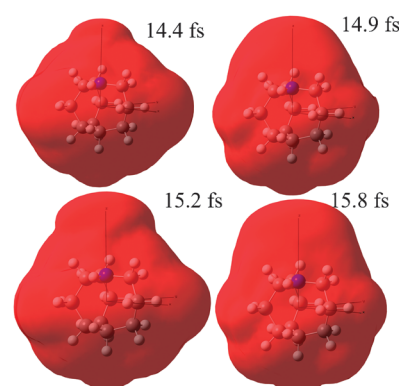


Fig. 8 Isocontours ($0.000055 |e| \text{\AA}^{-3}$) of $\rho(t)$ for the first four times shown in Fig. 7.

$0.000055 |e| \text{\AA}^{-3}$. While it is harder to observe the changes in these plots because of the multi configuration character of the excited states that are interfering to provide the density, one can clearly see that there are significant changes in the localization of the electron density with contours looking closer to that of the 2nd A state with an accumulation of electron density at 14.4 and 15.2 fs.

We show in Fig. 9 the populations in the excited states (top panel) and the oscillations of the dipole moment (lower panel) with a pulse with the same excitation wavelength of 0.18 a.u. but twice the duration of the one used in Fig. 4–6. The field strength has been reduced to 0.04 a.u. to keep the population in the excited states above the IP about 0.1%. The longer pulse allows to deplete more the GS and to access almost selectively the 2nd A state. This can be readily understood on the basis of the first order perturbation term of eqn (4). This leads to wider oscillations of the dipole $\mu(t)$ since there is a larger weight on the 2nd A state, which has a positive dipole moment along z (see Table 1).

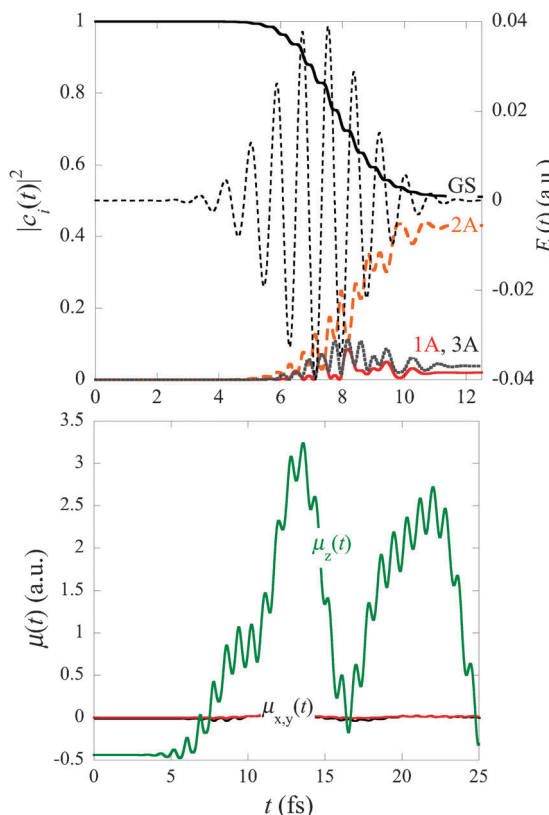


Fig. 9 Top: Time evolution of the weights, $|c_i(t)|^2$, eqn (3), on the excited states for a pulse polarized in the $+z$ direction ($\omega = 0.18$ a.u., $|E| = 0.04$ a.u., $\sigma = 60$ a.u. and $\phi = 0$ in eqn (2)). The pulse is shown in dashes, scale on the right. Only A states are populated by a pulse polarized in the z direction. Compared to Fig. 5, a longer pulse allows to more selectively populate the 2nd A state. Bottom: Time-dependence of the components of the dipole moment, $\mu(t)$ (eqn (6)).

We now turn to the stereodynamics induced by a pulse polarized in the x direction. Such a polarization gives access to both the E states by one-photon transitions and to A states by two-photon transitions from the excited E states. Because an exciting pulse polarized in the (x,y) plane gives access to excited states of a different symmetry than that of the GS with a higher oscillator strength, it is easier to control the dynamics with such a pulse. As can be seen from Fig. 10, a richer dynamics is therefore observed, even at a field strength lower than 0.05 a.u. For a field strength of 0.02 a.u. (1.4×10^{13} W cm $^{-2}$), a width of the envelope σ of 30 a.u. (0.72 fs) and a wavelength of 253 nm (top panel of Fig. 10), one essentially accesses the 1st excited E state, with a weight of 16.2% on one component of the E state and of 5.8% on the other, with a few percents of population in the second excited E state. All together, this corresponds to a depletion of the GS of 26.8%. The weights on the excited states are shown in Fig. 10. Note also the transient population to the first A state during the pulse which is due to two-photon processes. For this field strength, the population in the neutral states above the IP is reaching 0.1%. The results for a pulse twice longer and slightly weaker (0.015 a.u.) are essentially the same (lower panel of Fig. 10).

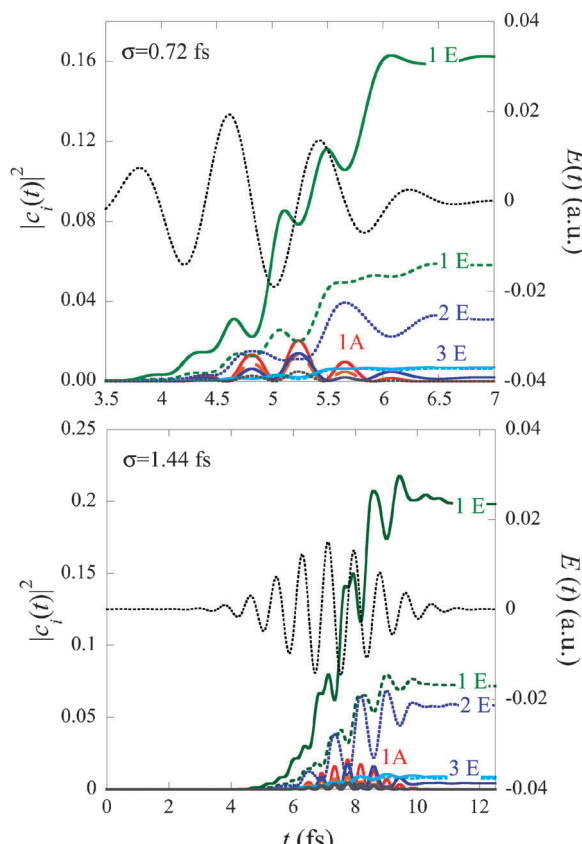


Fig. 10 Time evolution of the weights, $|c_i(t)|^2$, eqn (3), on the excited states for a pulse polarized in the $+x$ direction (top: $\omega = 0.18$ a.u., $|E| = 0.02$ a.u., $\sigma = 30$ a.u. and $\phi = 180^\circ$, bottom $\omega = 0.18$ a.u., $|E| = 0.015$ a.u., $\sigma = 60$ a.u. and $\phi = 180^\circ$ in eqn (2)). The pulse is shown in dashes, scale on the right. Only E states are significantly populated at the end of the pulse. There is no significant difference between the two durations of the pulse.

The time dependence of the three components of the dipole moment (eqn (6)) is given in Fig. 11 for the parameters of the short pulse ($\sigma = 0.72$ fs). The first oscillation of the x component is due to the beating between the GS and the 1st excited E state, while the slow modulation is due to the beating between the 1st and the 2nd excited E states. Since the pulse polarized in x excites the component of the E state better aligned with x (see Table 1 and Fig. 3), the beating with the GS is not very much present in the y component of the dipole. We also note a small oscillation of the dipole along z , which is due to the small component of the dipole moment of the E states along the z direction.

The time-dependence of the dipole reflects that of the one electron density since the dipole can also be written as a mean value on $\rho(t)$. Isocontours of $\rho_{\text{GS}}(0) - \rho(t)$ are shown in Fig. 12 for the values of time where the dipole along x is maximum and minimum (shown as filled circles in Fig. 11). Since for the first E state, the main configurations are an excitation from the MO 43 to the MO 45, see Fig. 2, when we plot the difference $\rho_{\text{GS}}(0) - \rho(t)$, we mainly visualize the changes along the x direction. The electron density is oscillating in the positive and negative x directions. A similar picture, not shown, is obtained in the y direction but with a smaller amplitude motion of the electronic density.

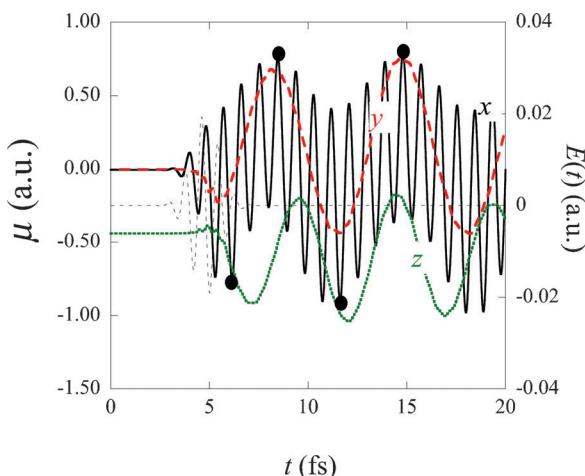


Fig. 11 Time-dependence of the components of the dipole moment, $\mu(t)$ (eqn (6)) computed for the pulse used in Fig. 10 top panel. The x -component is given by the (black) full line, the y -component by the dashed (red) line, and the z -component by the (green) dotted line. The fast beating of the x -component is due to the beating between the GS and the component of the 1st E state most aligned with x . There is also a smaller population in the other component of the E state whose transition dipole has a smaller component along x and which is better aligned with y . The full circles show the times at which isocontours of the electron density, $\rho(t)$ are shown in Fig. 10 below. The pulse is shown in dashes, scale on the right.

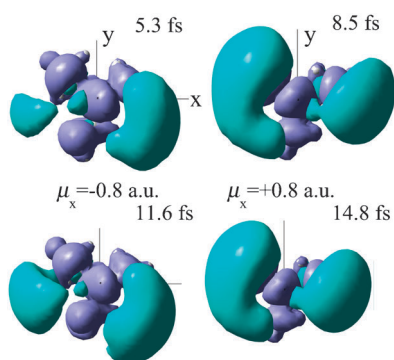


Fig. 12 Time-dependence of the difference $\rho_{\text{GS}} - \rho(t)$ (isocontour value $0.0001 |e| \text{ \AA}^{-3}$) at the times shown in Fig. 11 where the component of the dipole along x is equal to -0.8 a.u and $+0.8$ a.u. respectively.

Taking an IR frequency (800 nm) and a duration of the pulse at $\sigma = 0.60$ fs reduces the number of oscillations in the envelope to one cycle. We define $\mathbf{E}(t)$ from the derivative of the vector potential $\mathbf{A}(t)$.⁵⁹ The weights on the excited states for a non-resonant excitation with a field strength of 0.03 a.u., and maintaining the polarization in the x -direction, are shown in Fig. 13 for two values of the CEP phase (see eqn (2)), $\phi = 0^\circ$ (top) and $\phi = 180^\circ$ (bottom). Compared to Fig. 10 (top panel for the short pulse) which was computed for a resonant excitation, the total amount of excitation to the first E state does not vary significantly for both CEP values and remains about 20%. However, several other excited states, of A and E symmetry, now contribute about 5%, which leads to a larger depletion of the GS, which here reaches 72%. In particular, a slightly larger population remains in the A states at the end of

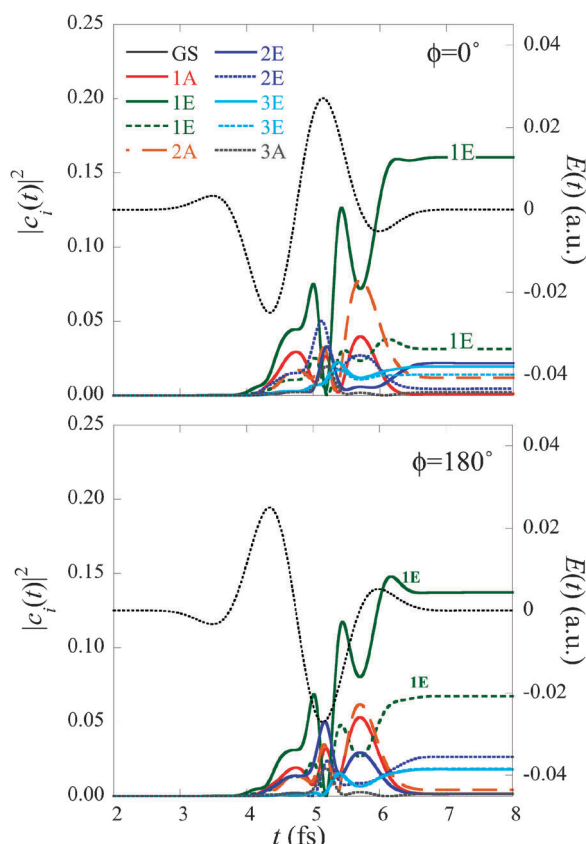


Fig. 13 Time evolution of the weights, $|c_i(t)|^2$, eqn (3), on the excited states for a non resonant pulse polarized in the $+x$ direction ($|E| = 0.03$ a.u., $\omega = 0.056$ a.u., $\sigma = 25$ a.u. and $\phi = 0$ (top) and 180° (bottom) in eqn (2)). The pulse is shown in dotted lines. The pulse is computed as the derivative of the vector potential $d\mathbf{E}/dt = (-1/c)d\mathbf{A}(t)/dt$. Note how different components of the second E state are accessed for the two values of the CEP phase. The 1st E state is the most populated at the end of the pulse. For the $\phi = 0^\circ$ pulse, one access selectively the first component of the 1st E state (labeled A component in Fig. 3).

the pulse, namely 0.1% in the 1st excited A state, 1.2% in the 2nd A state and 0.2% in the 3rd A state. The rest of the excited population is in the 2nd (2.5%) and 3rd (2.5%) excited E states. For this field strength too, there is less than 0.12% of excitation in the neutral states that lie above the IP. Note also the significant transient excitation of the 1st and 2nd A state that reach about 4% and 8% and that are accessed in phase in the second half of the pulse since it is a two-photon transition.

Changing the CEP to 180° (Fig. 13, bottom panel) increases the amount of excitation in the y component of the 1st excited E state from 3% for $\phi = 0^\circ$ (top) to about 8% for $\phi = 180^\circ$ CEP (bottom), but otherwise leads to similar weights on the excited states at the end of the pulse. The early dynamics during the pulse is however quite different for the two values of the CEP phase. This is due to the access of the different components of the second excited E state at the very beginning of the pulse for the two values of the CEP phase = 0. This selectivity leads to charge migration initially going in opposite directions along the x axis, as shown in Fig. 14 and 15. We note that these effects may not be easy to observe

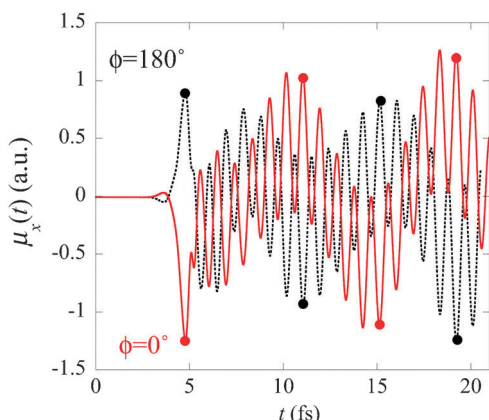


Fig. 14 The time evolution of $\mu_x(t)$ for the non resonant excitation pulses used in Fig. 13, $\phi = 0^\circ$ (full line) and $\phi = 180^\circ$ (dotted line). One can see that the dipole continues to oscillate with opposite phases after the pulse ended ($t > 6$ fs). The full circles correspond to the time values for which the electron density is computed in Fig. 15.

experimentally, since orientation of the molecule along the y -axis is likely to be very difficult.

Fig. 14 shows the time evolution of the x component of the time dependent dipole for the two values of the CEP phase. At the beginning of the pulse, the dipole along x varies in opposite directions and continues to oscillate with opposite phases. This is due to the fact different components of the 2nd E state are accessed during the first half cycle of the pulse, see Fig. 13.

The corresponding differences in the densities, $\rho_{GS}(0) - \rho(t)$, are shown in Fig. 15. One clearly sees that varying the CEP phase by 180° corresponds to an accumulation of charge in opposite directions along the x axis. This is due to the fact that at short time, there is transient population in the different

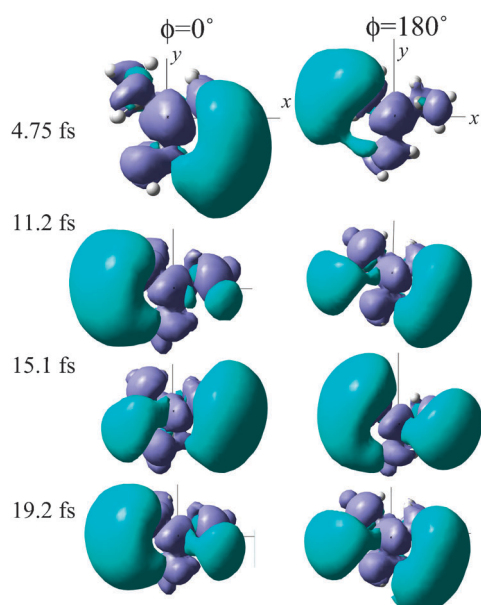


Fig. 15 Isocontours of the difference $\rho_{GS} - \rho(t)$, (isocontour value $0.0001 |e|/\text{\AA}^3$) computed for the times shown in Fig. 14. One clearly sees that the accumulation of negative charge occurs at opposite values of x , in agreement with the opposite values of the dipole moment.

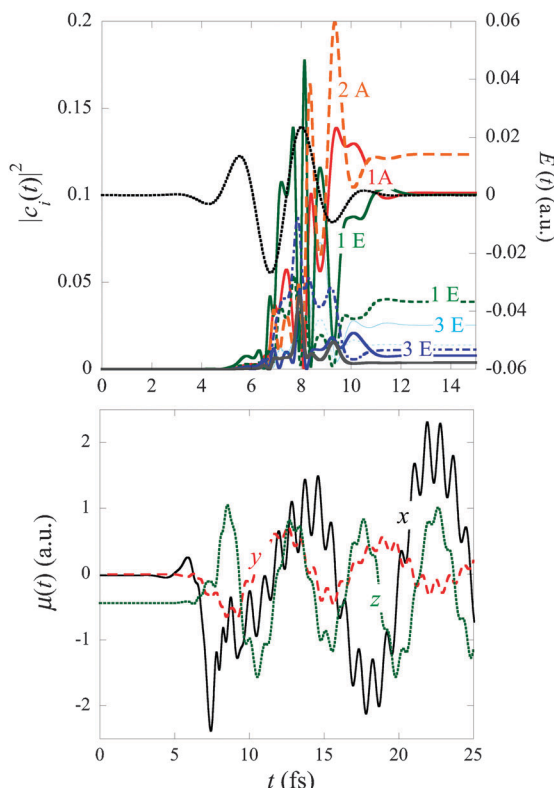


Fig. 16 Top: Time evolution of the weights, $|c_i(t)|^2$, eqn (3), on the excited states for a non resonant pulse polarized in the $+x$ direction ($|E| = 0.028$ a.u., $\omega = 0.056$ a.u., $\sigma = 60$ a.u. and $\phi = 0$ (top) in eqn (2)). The pulse is shown in dotted lines. Compared to the top panel of Fig. 13, a longer pulse leads to a much higher population in the excited A states. Bottom: Time-dependence of the components of the dipole moment, $\mu(t)$ (eqn (6)). The x -component is given by the (black) full line, the y -component by the dashed (red) line, and the z -component by the (green) dotted line. The complexity of the time evolution of the components of the dipole reflects the complex superposition of states that is built at the end of the pulse.

components of the 2nd excited E state for the two values of CEP.

When a longer excitation pulse is used, with a $\sigma = 1.44$ fs (about twice the duration of the results shown in Fig. 13–15), there is more than one cycle in the envelope of the pulse and the multi photon excitation produces a much richer electron dynamics. The results are shown in Fig. 16, where in addition to a longer duration, the strength of the electric field was reduced to 0.028 a.u., to keep the population in the excited states above the IP to 0.1%. The weights on the excited states are shown in the top panel. There is now more population in the A states (10% in the 1st A state and 12% in the 2nd one) than in the E states (14% in total for the 1st E state and 2% in the 2nd E). The GS is now depleted to 57%. As a consequence, the time evolution of the x , y and z components of the dipole, $\mu(t)$ (lower panel of Fig. 16) is much more complex.

To conclude this section about results, we show that it is possible to populate selectively one of the component of the first E state by aligning the polarization of the pulse in the (x,y) plane with a given component of the E state,

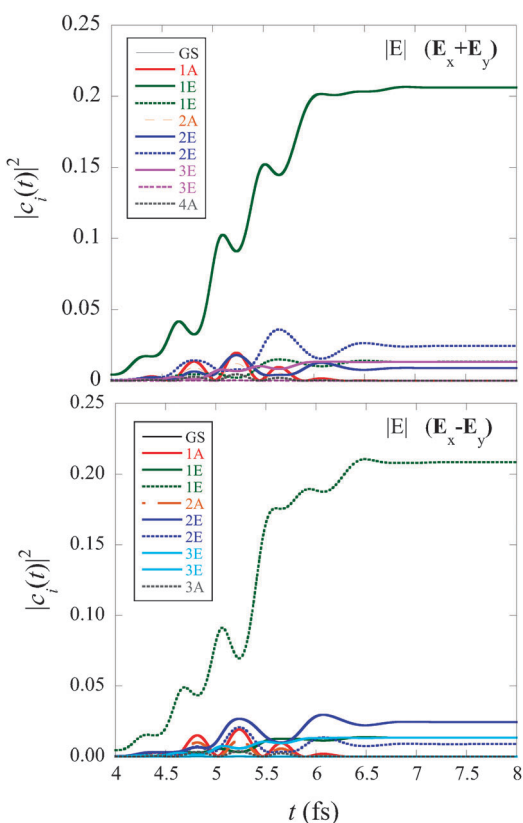


Fig. 17 Time evolution of the weights, $|c_i(t)|^2$, eqn (3), on the excited states for a resonant pulse polarized in the (x,y) plane ($|E| = 0.02$ a.u., $\omega = 0.18$ a.u., $\sigma = 30$ a.u. and $\phi = 0$ in eqn (2)). Top panel, the polarization is $E_x + E_y$ and it is the component of the first E state labeled A in Fig. 3 that is accessed while for $E_x - E_y$, bottom panel, it is the component labeled B in Fig. 3 that is selectively accessed.

Fig. 17. In the case of the first E state, it amounts to rotate the electric field at 45° in the (x,y) plane. This can be inferred from the plot of the density of the two components of the E state shown in Fig. 3.

6. Concluding remarks

ABCU, ($C_{10}H_{19}N$), is an 86 electron medium sized cage-like polyatomic molecule with nine dipole allowed excited states below the onset of vertical ionization, (at a low potential of 6.96 eV computed at the B3LYP level, expt'l 7.01). We computed the electronic structure, energetics and dynamics in a many electron formalism for excitation by one or few optical cycle laser pulses. The results allowed us to demonstrate selective stereodynamics in the excited states of the neutral at the computational level. The basis for selectivity is that the electronic density in the excited states is polarized along the different principal axes of the cage. This is reflected by the value of the components of the permanent dipole moments in the excited states. The ultrashort electronic reorganization following a few-cycle pulse can be monitored by including the laser field as part of the Hamiltonian. The short polarized pulse builds a coherent superposition of excited states with a non-stationary localized electronic density. The oscillations of the non-stationary coherent

electronic state are studied through the numerical solution of the time-dependent Schrödinger equation in a rather large electronic basis set. The migration of charge along the molecular cage as well as the time-alternation of the dipole moment of the molecule are exhibited. It can be controlled by the polarization of the light thereby giving rise to stereodynamic effects. The electronic coherence survives well after the light field is over. Another useful control parameter is the phase shift between the carrier wave of the light and its time-envelope. Thereby alignment of the electronic density can be achieved. The rigidity of the molecular cage is maintained during electronic excitation and for a time window of several fs after the short pulse is over so that one can excite and probe the purely electronic dynamics prior to the onset of nuclear motion.

At higher intensities and to a rather limited extent at the field strengths used in this study, we expect ionization to occur both by tunnel and multiphoton processes, as can be qualitatively judged from the values of the Keldysh parameters reported above. Work is in progress to include the ionization continua in the formalism. Experimentally, special techniques will therefore be needed to conclusively probe the selectivity of the dynamics in the excited states of the neutral. Techniques to do so may involve the correlated detection of multiple neutral and ionic fragments, for instance making judicious use of reaction microscopes,⁷⁰ and/or the use of very short wavelength (XUV or X-ray) radiation. The latter would allow probing of the ultrafast electron dynamics by means of the production of photoelectrons or ionic fragments with kinetic energies that are not produced by the pump laser pulse. Experiments along these lines in molecules with the complexity of ABCU have yet to be undertaken, but have recently been successfully performed in small, diatomic molecules like H_2 , O_2 and N_2 .^{71,72}

Acknowledgements

BM is a Research Fellow and FR is Director of Research of FNRS-Belgium. This work was partially supported by the James Franck program for Laser-Matter interaction and by the EC FET proactive STREP project MOLOC.

References

- P. Agostini and L. F. DiMauro, *Rep. Prog. Phys.*, 2004, **67**, 813–855.
- P. B. Corkum and F. Krausz, *Nat. Phys.*, 2007, **3**, 381–387.
- M. F. Kling and M. J. J. Vrakking, *Annu. Rev. Phys. Chem.*, 2008, **59**, 463–492.
- F. Krausz and M. Ivanov, *Rev. Mod. Phys.*, 2009, **81**, 163–234.
- M. Drescher, M. Hentschel, R. Kienberger, M. Uiberacker, V. Yakovlev, A. Scrinizi, T. Westerwalbesloh, U. Kleineberg, U. Heinzmann and F. Krausz, *Nature*, 2002, **419**, 803–807.
- M. Uiberacker, T. Uphues, M. Schultz, A. J. Verhoeft, V. Yakovlev, M. F. Kling, J. Rauschenberger, N. M. Kabachnik, H. Schroder, M. Lezius, K. L. Kompa, H. G. Muller, M. J. J. Vrakking, S. Hendel, U. Kleineberg, U. Heinzmann, M. Drescher and F. Krausz, *Nature*, 2007, **446**, 627–632.
- A. L. Cavalieri, N. Muller, T. Uphues, V. S. Yakovlev, A. Baltuska, B. Horvath, B. Schmidt, L. Blumel, R. Holzwarth, S. Hendel, M. Drescher, U. Kleineberg, P. M. Echenique,

- R. Kienberger, F. Krausz and U. Heinzmann, *Nature*, 2007, **449**, 1029–1032.
- 8 G. Sansone, F. Kelkensberg, J. F. Perez-Torres, F. Morales, M. F. Kling, W. Siu, O. Ghafur, P. Johnsson, M. Swoboda, E. Benedetti, F. Ferrari, F. Lepine, J. L. Sanz-Vicario, S. Zherebtsov, I. Znakovskaya, A. L'Huillier, M. Y. Ivanov, M. Nisoli, F. Martin and M. J. J. Vrakking, *Nature*, 2010, **465**, 763–766.
- 9 H. Niikura, F. Legare, R. Hasbani, M. Y. Ivanov, D. M. Villeneuve and P. B. Corkum, *Nature*, 2003, **421**, 826–829.
- 10 J. Itatani, J. Levesque, D. Zeidler, H. Niikura, H. Pepin, J. C. Kieffer, P. B. Corkum and D. M. Villeneuve, *Nature*, 2004, **432**, 867–871.
- 11 O. Smirnova, Y. Mairesse, S. Patchkovskii, N. Dudovich, D. Villeneuve, P. Corkum and M. Y. Ivanov, *Nature*, 2009, **460**, 972–977.
- 12 S. Baker, J. S. Robinson, C. A. Haworth, H. Teng, R. A. Smith, C. C. Chirila, M. Lein, J. W. G. Tisch and J. P. Marangos, *Science*, 2006, **312**, 424–427.
- 13 M. F. Kling, C. Siedschlag, A. J. Verhoef, J. I. Khan, M. Schultze, T. Uphues, Y. Ni, M. Uiberacker, M. Drescher, F. Krausz and M. J. J. Vrakking, *Science*, 2006, **312**, 246–248.
- 14 I. Znakovskaya, P. von den Hoff, S. Zherebtsov, A. Wirth, O. Herrwerth, M. J. J. Vrakking, R. de Vivie-Riedle and M. F. Kling, *Phys. Rev. Lett.*, 2009, **103**, 103002–103004.
- 15 B. K. McFarland, J. P. Farrell, P. H. Bucksbaum and M. Guhr, *Science*, 2008, **322**, 1232–1235.
- 16 S. Haessler, J. Caillat, W. Boutu, C. Giovanetti-Teixeira, T. Ruchon, T. Auguste, Z. Diveki, P. Breger, A. Maquet, B. Carre, R. Taieb and P. Salieres, *Nat. Phys.*, 2010, **6**, 200–206.
- 17 H. J. Wörner, J. B. Bertrand, D. V. Kartashov, P. B. Corkum and D. M. Villeneuve, *Nature*, 2010, **466**, 604–607.
- 18 W. Li, A. A. Jaróñ-Becker, C. W. Hogle, V. Sharma, X. Zhou, A. Becker, H. C. Kapteyn and M. M. Murnane, *Proc. Natl. Acad. Sci. U. S. A.*, 2010, **107**, 20219–20222.
- 19 M. Meckel, D. Comtois, D. Zeidler, A. Staudte, D. Pavicic, H. C. Bandulet, H. Pepin, J. C. Kieffer, R. Dorner, D. M. Villeneuve and P. B. Corkum, *Science*, 2008, **320**, 1478–1482.
- 20 H. Akagi, T. Otobe, A. Staudte, A. Shiner, F. Turner, R. Dorner, D. M. Villeneuve and P. B. Corkum, *Science*, 2009, **325**, 1364–1367.
- 21 Y. Huismans, A. Rouzée, A. Gijsbertsen, J. H. Jungmann, A. S. Smolkowska, P. S. W. M. Logman, F. Lépine, C. Cauchy, S. Zamith, T. Marchenko, J. M. Bakker, G. Berden, B. Redlich, A. F. G. van der Meer, H. G. Müller, W. Vermin, K. J. Schafer, M. Spanner, M. Y. Ivanov, O. Smirnova, D. Bauer, S. V. Popruzhenko and M. J. J. Vrakking, *Science*, 2010, **331**, 61, DOI: 10.1126/science.1198450.
- 22 M. Yamashita, K. Yamane and R. Morita, *IEEE J. Sel. Top. Quantum Electron.*, 2006, **12**, 213–222.
- 23 E. Matsubara, K. Yamane, T. Sekikawa and M. Yamashita, *J. Opt. Soc. Am. B*, 2007, **24**, 985–989.
- 24 F. Reiter, U. Graf, M. Schultze, W. Schweinberger, H. Schroder, N. Karpowicz, A. M. Azzeer, R. Kienberger, F. Krausz and E. Goulielmakis, *Opt. Lett.*, 2010, **35**, 2248–2250.
- 25 O. Ghafur, A. Rouzee, A. Gijsbertsen, W. K. Siu, S. Stolte and M. J. J. Vrakking, *Nat. Phys.*, 2009, **5**, 289–293.
- 26 L. Holmegaard, J. H. Nielsen, I. Nevo, H. Stapelfeldt, F. Filsinger, J. Kupper and G. Meijer, *Phys. Rev. Lett.*, 2009, **102**, 02301.
- 27 H.-J. Werner and P. J. Knowles, *J. Chem. Phys.*, 1985, **82**, 5053–5063.
- 28 P. J. Knowles and H.-J. Werner, *Chem. Phys. Lett.*, 1985, **115**, 259–267.
- 29 H.-J. Werner, P. J. Knowles, F. R. Manby, M. Schuetz, P. Celani, G. Knizia, T. Korona, R. Lindh, A. Mitrushenkov, G. Rauhut, T. B. Adler, R. D. Amos, A. Bernhardsson, A. Berning, D. L. Cooper, M. J. O. Deegan, A. J. Dobbyn, F. Eckert, E. Goll, C. Hampel, A. Hesselmann, G. Hetzer, T. Hrenar, G. Jansen, C. Koeppl, Y. Liu, A. W. Lloyd, R. A. Mata, A. J. May, S. J. McNicholas, W. Meyer, M. E. Mura, A. Nicklass, P. Palmieri, K. Pflueger, R. Pitzer, M. Reiher, T. Shiozaki, H. Stoll, A. J. Stone, R. Tarroni, T. Thorsteinsson, M. Wang and A. Wolf, *MOLPRO a package of ab initio programs*, 2009, Cardiff, UK.
- 30 D. H. Aue, H. M. Webb and M. T. Bowers, *J. Am. Chem. Soc.*, 1975, **97**, 4136–4137.
- 31 V. Galasso, *Chem. Phys.*, 1997, **215**, 183–190.
- 32 A. M. Weber, A. Acharya and D. H. Parker, *J. Phys. Chem.*, 1984, **88**, 6087–6089.
- 33 M. J. Frisch, G. W. Trucks, H. B. Schlegel, G. E. Scuseria, M. A. Robb, J. R. Cheeseman, G. Scalmani, V. Barone, B. Mennucci, G. A. Petersson, H. Nakatsuji, M. Caricato, X. Li, H. P. Hratchian, A. F. Izmaylov, J. Bloino, G. Zheng, J. L. Sonnenberg, M. Hada, M. Ehara, K. Toyota, R. Fukuda, J. Hasegawa, M. Ishida, T. Nakajima, Y. Honda, O. Kitao, H. Nakai, T. Vreven, J. J. A. Montgomery, J. E. Peralta, F. Ogliaro, M. Bearpark, J. J. Heyd, E. Brothers, K. N. Kudin, V. N. Staroverov, R. Kobayashi, J. Normand, K. Raghavachari, A. Rendell, J. C. Burant, S. S. Iyengar, J. Tomasi, M. Cossi, N. Rega, J. M. Millan, M. Klene, J. E. Knox, J. B. Cross, V. Bakken, C. Adamo, J. Jaramillo, R. Gomperts, R. E. Stratmann, O. Yazyev, A. J. Austin, R. Cammi, C. Pomelli, J. W. Ochterski, R. L. Martin, K. Morokuma, V. G. Zakrzewski, G. A. Voth, P. Salvador, J. J. Dannenberg, S. Dapprich, A. D. Daniels, Ö. Farkas, J. B. Foresman, J. V. Ortiz, J. Cioslowski and D. J. Fox, *Gaussian 09, Revision A.1*, 2009, Gaussian, Inc., Wallingford CT.
- 34 H. Stapelfeldt and T. Seideman, *Rev. Mod. Phys.*, 2003, **75**, 543–557.
- 35 H. Sakai, C. P. Safvan, J. J. Larsen, K. M. Hilligsoe, K. Hald and H. Stapelfeldt, *J. Chem. Phys.*, 1999, **110**, 10235–10238.
- 36 F. Rosca-Pruna and M. J. J. Vrakking, *Phys. Rev. Lett.*, 2001, **87**, 153902.
- 37 F. Remacle and R. D. Levine, *Phys. Rev. A: At., Mol., Opt. Phys.*, 2011, **83**, 013411.
- 38 F. Kelkensberg, G. Sansone, M. Ivanov and M. J. J. Vrakking, *Phys. Chem. Chem. Phys.*, 2011, DOI: 10.1039/clcp20058e.
- 39 T. Kato and H. Kono, *Chem. Phys. Lett.*, 2004, **392**, 533–540.
- 40 T. Kato and H. Kono, *J. Chem. Phys.*, 2008, **128**, 184102–184108.
- 41 T. Kato and H. Kono, *Chem. Phys.*, 2009, **366**, 46–53.
- 42 T. T. Nguyen-Dang, M. Peters, S.-M. Wang, E. Sinelnikov and F. Dion, *J. Chem. Phys.*, 2007, **127**, 174107–174114.
- 43 T. T. Nguyen-Dang, M. Peters, S. M. Wang and F. Dion, *Laser Phys.*, 2009, **19**, 1521–1534.
- 44 J. Caillat, J. Zanghellini, M. Kitzler, O. Koch, W. Kreuzer and A. Scrinzi, *Phys. Rev. A: At., Mol., Opt. Phys.*, 2005, **71**, 012712.
- 45 G. Jordan, J. Caillat, C. Ede and A. Scrinzi, *J. Phys. B: At., Mol. Opt. Phys.*, 2006, **39**, S341–S347.
- 46 I. Barth, J. Manz and L. Serrano-Andres, *Chem. Phys.*, 2008, **347**, 263–271.
- 47 M. Nest, F. Remacle and R. D. Levine, *New J. Phys.*, 2008, **10**, 025019–025024.
- 48 F. Remacle, M. Nest and R. D. Levine, *Phys. Rev. Lett.*, 2007, **99**, 183902–183904.
- 49 A. D. Bandrauk, S. Chelkowski and H. S. Nguyen, *Int. J. Quantum Chem.*, 2004, **100**, 834–844.
- 50 K. Harumiya, H. Kono, Y. Fujimura, I. Kawata and A. D. Bandrauk, *Phys. Rev. A: At., Mol., Opt. Phys.*, 2002, **66**, 043403.
- 51 F. Remacle and R. D. Levine, *Proc. Natl. Acad. Sci. U. S. A.*, 2006, **103**, 6793–6798.
- 52 H. Hennig, J. Breidbach and L. S. Cederbaum, *J. Phys. Chem. A*, 2005, **109**, 409–414.
- 53 G. Periyasamy, R. D. Levine and F. Remacle, *Chem. Phys.*, 2009, **366**, 129–138.
- 54 F. Remacle and R. D. Levine, *Phys. Rev. A: At., Mol., Opt. Phys.*, 2011, **83**, 013411.
- 55 A. D. Bandrauk, S. Chelkowski, S. Kawai and H. Z. Lu, *Phys. Rev. Lett.*, 2008, **101**, 153901.
- 56 H. Kono, Y. Sato, N. Tanak, T. Kato, K. Nakai, S. Koseki and Y. Fujimura, *Chem. Phys.*, 2004, **304**, 203–226.
- 57 D. Geppert, P. von den Hoff and R. de Vivie-Riedle, *J. Phys. B: At., Mol. Opt. Phys.*, 2008, **41**, 074006.
- 58 B. H. Muskatel, F. Remacle and R. D. Levine, *Phys. Scr.*, 2009, **80**, 048101.
- 59 S. Chelkowski and A. D. Bandrauk, *Phys. Rev. A: At., Mol., Opt. Phys.*, 2002, **65**, 061802.
- 60 O. Smirnova, M. Spanner and M. Ivanov, *Phys. Rev. A: At., Mol., Opt. Phys.*, 2008, **77**, 033407.

- 61 K. Harumiya, H. Kono, Y. Fujimura, I. Kawata and A. D. Bandrauk, *Phys. Rev. A: At., Mol., Opt. Phys.*, 2002, **66**, 043403.
- 62 G. L. Kamta and A. D. Bandrauk, *Phys. Rev. A: At., Mol., Opt. Phys.*, 2007, **76**, 053409.
- 63 F. Kelkensberg, C. Lefebvre, W. Siu, O. Ghafur, T. T. Nguyen-Dang, O. Atabek, A. Keller, V. Serov, P. Johnsson, M. Swoboda, T. Remetter, A. L'Huillier, S. Zherebtsov, G. Sansone, E. Benedetti, F. Ferrari, M. Nisoli, F. Lepine, M. F. Kling and M. J. J. Vrakking, *Phys. Rev. Lett.*, 2009, **103**, 123005.
- 64 S. Klinkusch, P. Saalfrank and T. Klamroth, *J. Chem. Phys.*, 2009, **131**, 114304–114308.
- 65 S. Sukiasyan, S. Patchkovskii, O. Smirnova, T. Brabec and M. Y. Ivanov, *Phys. Rev. A: At., Mol., Opt. Phys.*, 2010, **82**, 043414.
- 66 X.-B. Bian and A. D. Bandrauk, *Phys. Rev. Lett.*, 2010, **105**, 093903.
- 67 A. Guldberg, *Chem. Phys. Lett.*, 1989, **154**, 487–491.
- 68 R. McWeeny, *Proc. R. Soc. London, Ser. A*, 1959, **253**, 242–249.
- 69 R. McWeeny and B. T. Sutcliffe, *Methods of Molecular Quantum Mechanics*, Academic Press, London, 1969.
- 70 J. Ullrich, R. Moshammer, A. Dorn, R. Dorner, L. P. H. Schmidt and H. Schnidt-Bocking, *Rep. Prog. Phys.*, 2003, **66**, 1463–1545.
- 71 F. Kelkensberg, W. Siu, J. F. Pérez-Torres, F. Morales, G. Gademann, A. Rouzée, P. Johnsson, M. Lucchini, F. Calegari, J. L. Sanz-Vicario, F. Martin and M. J. J. Vrakking, 2011, submitted.
- 72 W. Siu, F. Kelkensberg, G. Gademann, A. Rouzee, P. Johnsson and M. J. J. Vrakking, 2011, in preparation.